Korean J. Chem. Eng., 39(4), 1020-1027 (2022)
DOI: 10.1007/s11814-021-0968-0

pISSN: 0256-1115
eISSN: 1975-7220

High-performance ZIF-302 mixed-matrix membranes for efficient CO_2 capture

Junfeng Qian*, Eryue Song, Haiqian Lian**, Jinlong Jiang***, Chongqing Wang**,†, and Yichang Pan**,†**

*Jiangsu Province Key Laboratory of Fine Petrochemical Engineering, Changzhou University, Changzhou, Jiangsu, China
**State Key Laboratory of Materials-Oriented Chemical Engineering, College of Chemical Engineering, Nanjing Tech University, Nanjing, Jiangsu, China
***Key Laboratory for Palygorskite Science and Applied Technology of Jiangsu Province, Faculty of Chemical Engineering, Huaiyin Institute of Technology, Huaian, 223003, China
(*Received 3 August 2021 • Revised 27 September 2021 • Accepted 29 September 2021*)

Abstract−High-performance mixed matrix membranes (MMMs) were developed to assist in controlling global warming by capturing carbon dioxide (CO_2) from moist flue gas. However, the separation performance of MMMs has always been limited by gas permeability and long-term operating stability under humid conditions. ZIF-302 is a novel chabazite (CHA) topology structure with hydrophobic ligand. Herein, uniform ZIF-302 nanocrystals were doped into the P84 polymer matrix to synthesize different content of defect-free ZIF-302/P84 MMMs for CO_2/N_2 separation. A significant combination of gas permeability and separation factors was found in MMMs with a ZIF-302 packing load of 30 wt%. The gas permeability of CO_2 and the separation factor of CO_2/N_2 were significantly increased to 5.2 Barrers and 46, respectively, which breaks the trade-off between permeability and selectivity of the polymer membrane. In addition, the long-term operation stability showed that the separation performance of ZIF-302/P84 MMMs for CO_2/N_2 was maintained more than 30 h at 3 bar and 60 °C. The main characteristics of the MMMs prepared in this paper include the combination of favorable structural stability under humid conditions and unaffected CO_2/N_2 gas separation performance.

Keywords: Mixed-matrix Membranes, MOFs, ZIF-302, Gas Separation, CO_2 Capture

INTRODUCTION

Carbon dioxide is considered a major contributor to greenhouse gas emissions, and its increasing concentration in our atmosphere could be leading to serious global warming [1,2]. CO_2 is also one of the main impurities in natural gas, which needs to be separated before the gas is sent to the pipeline to prevent serious corrosion problems. Therefore, it is important to develop a process that can effectively separate and recover carbon dioxide from these different natural gas sources [3]. Membrane separation based on CO_2 capture is considered as a promising alternative to conventional separation, mainly due to its higher energy efficiency and reliability. Polymer membranes have dominated commercial gas separation due to their low cost, processibility, and excellent mechanical properties. However, they are constrained by a trade-off between permeability and selectivity, known as the Robertson upper bound [4], which passively affects their large-scale utility.

Mixed-matrix membranes (MMMs) are emerging gas separation membranes in recent years. It is a promising membrane structure composed of polymers and inorganic microporous materials which can overcome the above-mentioned limitations of the original polymer membranes [5-7]. However, conventional porous materials [8-11], such as zeolite and carbon molecular sieves, mostly have poor interface compatibility with the polymer matrix. Compared with traditional molecular sieve packing, MOFs have higher adsorption capacity, higher specific surface area, pore volume, and adjustable pore size. The presence of organic ligands in MOFs leads to better compatibility with the polymer matrix [12,13] and allows to increase the loading of inorganic fillers in the mixed-matrix membrane. MOF-based MMMs have been proven to be successfully applied in CO_2 capture [14], H_2 purification [12,15], CH_4 upgrading [16,17] and olefin/paraffin separation [18-20].

Many studies have proved that the doping of porous inorganic particles in polymers can significantly improve the gas permeation flux and separation performance of polymer membranes. Bae and colleagues used the traditional solution casting method to dope ZIF-90 into the 6FDA-DAM polymer membrane. The composite membrane showed excellent performance in separating CO_2/CH_4 mixed systems, exceeding the Robeson upper bound in 2008 [4]. Li's group prepared an ultra-thin ZIF-7/Pebax1657 composite membrane with a thickness of less than 500 nm, which showed an amazing separation effect in a CO_2/N_2 separation system [21]. In addition, Xiang and co-workers demonstrated that natural clay attapulgite (ATP) can be used as an effective filler to improve the performance of pure Pebax1657 membranes, including CO_2 permeability and CO_2/N_2 selectivity [22]. However, the separation performance of MMMs has always been limited by gas permeability and long-term operating stability under humid conditions. Therefore, the successful preparation of high stability mixed-matrix membranes and improving the gas permeability is highly desirable.

A novel chabazite (CHA) topology ZIF-302 structure with hydrophobic properties was developed by Yaghi and co-workers [23].

†To whom correspondence should be addressed.
E-mail: cqw@njtech.edu.cn, panyc@njtech.edu.cn

It is composed of zinc (II) salt with 2-methylimidazole (mIm) and 5-methylbenzimidazole (mbIm) by solvothermal reaction. Interestingly, ZIF-302 crystals exhibited excellent chemical stability, which was attributed to the large hydrophobic chain of 5-methylbenzimidazole in the material framework, and shows permanent microporosity with a narrow size of the pores (~3.5 Å). In addition, it has been reported that ZIF-302 shows significantly higher adsorption capacity and affinity for CO_2 than N_2, enabling effective dynamic separation of CO_2 from N_2. Moreover, ZIF-302 has no performance loss in several adsorption and desorption cycles as an adsorbent and can be easily regenerated by purging N_2 flow at room temperature [23,24]. Based on these attractive characteristics, it is expected that ZIF-302 may be the most promising membrane material for CO_2 capture.

In this work, native ZIF-302 nanocrystals were uniformly dispersed into P84 polymer matrix to prepare high-performance MMMs via the solution-blending method. The hydrophobic ZIF-302 nanocrystals with uniform particle size distribution were synthesized by introducing a modulator to be suitable for the preparation of MMMs. Simultaneously, Polyimide P84 was considered as a suitable polymer matrix because of its high thermal stability, antiplasticizing properties and good solubility in most polar solvents [25]. Therefore, various physical techniques (XRD, ATR-FTIR, TGA, SEM and DSC) were adopted to probe the microstructure of the as-synthesized ZIF-302/P84 MMMs. Furthermore, ZIF-302/P84 MMMs with higher CO_2/N_2 ideal selectivity were obtained by determining the optimum loading amount of nano-filler. The separation performance and long-term operating stability were systematically studied under dry and wet gas feed conditions. Therefore, the prepared high-performance ZIF-302/P84MMMs showed important research significance for improving gas permeability and long-term operation stability.

MATERIALS AND METHODS

1. Materials

Commercial co-polyimide P84 powder was purchased from Sinopharm Chemical Reagent Co. Ltd. Zinc nitrate hexahydrate ($Zn(NO_3)_2 \cdot 6H_2O$, 99%), sodium formate (HCOONa, 99%), 2-methylimidazole ($C_4H_6N_2$, 98%,) and 5-methylbenzimidazole ($C_8H_8N_2$, 99%) were obtained from Sigma-Aldrich. Methanol (CH_3OH, 99%), N,N-dimethylformamide (DMF, 98%) and N-Methyl pyrrolidone (NMP, 98%) were purchased from Sinopharm Chemical Reagent Co., Ltd. All purchased chemicals were used directly without further purification.

2. Synthesis of ZIF-302 Crystals

ZIF-302 nanocrystals were prepared by using the procedure reported in the literature with some modifications [26]. Briefly, the particles were prepared by dissolving $Zn(NO_3)_2 \cdot 6H_2O$ (2.8 mmol), 2-methylimidazole (2.4 mmol), and 5-methylbenzimidazole (2.8 mmol) in a 80 mL mixture of distilled water (20 mL) and DMF (60 mL) in a 100 mL vial and sonicating for 30 min. Subsequently, 1.6 mmol sodium formate was also added into the mixture solution at room temperature. The prepared solution was heated in the blast drying oven at 100 °C for 24 h, and the synthetic particles were washed with fresh methanol to obtain pure ZIF-302 nanocrystals. Subsequently, the product was dried in a vacuum oven at 160 °C for 10 h to obtain the ZIF-302 crystals.

3. Fabrication of ZIF-302/P84 MMMs

The ZIF-302/P84 MMMs were fabricated by using the solution-blending method. The weighed ZIF-302 nanocrystals were first dispersed in 2 mL of NMP solvent and ultrasound for 10 min to obtain a uniformly dispersed solution. The P84 base solution was also fabricated by dispersing 1 g P84 in 10 mL NMP solvent and then vigorously agitating at 35 °C for 14 h to obtain a thick viscous solution. Then, the hybrid membranes with the different contents of the ZIF-302 crystals were fabricated by combining with the above two solutions together in a glass bottle and stirring at a constant speed for 24 h until obtaining a thick viscous solution. Finally, the viscous solution was distributed on a clean glass plate and hybrid membrane was obtained by knife casting. The solvent in the membrane was slowly evaporated at room temperature for 20 h. The cast membrane was peeled off the glass plate and placed in a vacuum oven at 160 °C to dry completely.

4. Characterization

X-ray diffraction (XRD) peak patterns of synthetic particles were captured at room temperature using CuKα radiation (λ=1.54059 Å) at 40 kV and 40 mA with 2θ range of 3-45° on a Rigaku SmartLab TM 9 KW powder diffractometer. Nitrogen adsorption-desorption isotherms of nanoparticles were obtained at 77 K using a BELSORP machine. The specific surface areas of as-synthetic particles were calculated by the multipoint BET method based on the adsorption data, and the pore size distribution was estimated by the H-K method. Simultaneously, the as-synthetic particles were dried in a vacuum at 200 °C for 8 h prior to testing. The total pore volume was estimated by the maximum adsorption capacity of nitrogen gas at partial pressure (P/P_0=0.999). Adsorption equilibrium of N_2 and CO_2 on ZIF-302 crystals was obtained on Micromeritics ASAP 2020 apparatus at low pressure (up to 1 bar) and 298 K. Morphologies of as-synthetic crystals and MMMs were all measured with scanning electron microscope (SEM, Japan, Hitachi, S4800). Fourier transform infrared spectrometer (FTIR) spectra of MMMs were obtained (4,000-500 cm^{-1}) on the Nicolet IS 10 to verify that the crystals in the polymer matrix had been completely doped. Thermogravimetric analysis (TGA) of MMMs was obtained by using the Netzsch STA 449 thermal analysis system in the air atmosphere from 100 to 700 °C at a ramping rate of 20 °C/min. The glass transition temperature (T_g) of various loads MMMs was measured by using a differential scanning calorimeter (NETZSCH DSC 204 F1 Phoenix).

5. Gas Separation Test

CO_2/N_2 mixture permeation experiments were performed by the permeation setup reported in the literature [27]. A home-made permeation cell was applied for all gas tests and the permeation test conditions were fixed as 3 bar and 60 °C. Unless otherwise specified, the CO_2/N_2 mixed gas composition was 50/50 vol%, and the flow rate was fixed at 60 mL/min. Nitrogen (20 mL/min) was used as sweep gas for the permeate stream (atmospheric). The transmembrane pressure was adjusted in the range of 3 bar using a backpressure controller on the retention side. In all tests, the stage-cut less than 1% was maintained to avoid concentration polarization. The compositions of steady feed, retention and permeate were determined by gas chromatography (Agilent 7890). Residual gas

in the membrane and pipeline was removed by the vacuum pump prior to testing. To ensure the reliability of testing, three repeated membrane samples prepared under the same conditions were applied for the gas permeation, and the results were averaged as the final data with deviation. The steady-state permeability of gas i, P_i, is defined as follows [28]:

$$P_i = \frac{LN_i}{A(f_{R,i} - f_{P,i})} \quad (1)$$

where L is the thickness of the mixed matrix membrane (cm), estimated with a digital micrometer (Mitutoyo, Japan), N_i is the volume flow rate of gas i (cm^3/s), A is the effective area of membrane (cm^2), and f_R and f_P are the fugacity of retention and permeability (cmHg). The unit of the membrane permeability (P_i) is usually expressed as Barrer (1 Barrer=10^{-10} cm^3 (STP) cm/(cm^2 s cmHg)). The gas fugacity (i) was calculated using the following equation:

$$f_i = \emptyset_i x_i p \quad (2)$$

where the gas fugacity coefficient $\emptyset_i$ was calculated by the Redlich-Kwong-Soave equation using Aspen Plus [29], x_i is the molar fraction of component *i*, and p representes the gas total pressure. The separation factor ($\alpha_{i/j}$) for CO_2/N_2 mixture permeation was estimated by the following equation:

$$\alpha_{i/j} = \frac{P_i}{P_j} \quad (3)$$

RESULTS AND DISCUSSION

1. Synthesis of ZIF-302 Nanocrystals

Fig. 1 shows the XRD patterns and SEM images of the synthesized ZIF-302 nanocrystals. They were synthesized by adding an appropriate amount of sodium formate to the crystal synthesis solution. The XRD characterization results show that the synthesized sample exhibits some sharp diffraction peaks at 2θ about 5°, 8°, and 17°, which is well coincident with the simulated ZIF-302 structure reported in the literature [26]. As shown in Fig. 1(a), the pure phase ZIF-302 crystals were successfully prepared. The morphology of synthesized samples was found to be cubic by SEM characterization. Note that the synthesized crystals particularly easily agglomerate together and possess a large particle size if the appropriate amount of formate is not added [30]. Therefore, sodium formate plays a role in accelerating the nucleation rate of crystals in this paper, promoting the formation of homogeneous nanocrystals with smaller size [31,32]. The ZIF-302 crystals exhibit a well-defined size distribution with an average size of about 200-300 nm (Fig. 1(b)). The synthetic sample is more suitable to be used as a filler for the preparation of high-quality mixed matrix membranes compared to the large size and easy agglomeration crystals, which is mainly due to optimal particle size and mono-dispersity.

The microporosity of ZIF-302 nanocrystals was verified by nitrogen adsorption-desorption experiments at 77 K and 1bar. The syn-

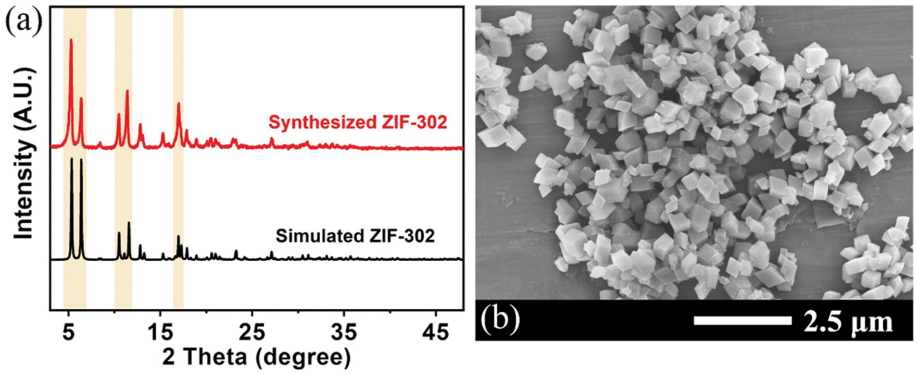

Fig. 1. (a) XRD patterns and (b) SEM images of the as-synthesized ZIF-302 nanoparticles at 100 °C for 24 h.

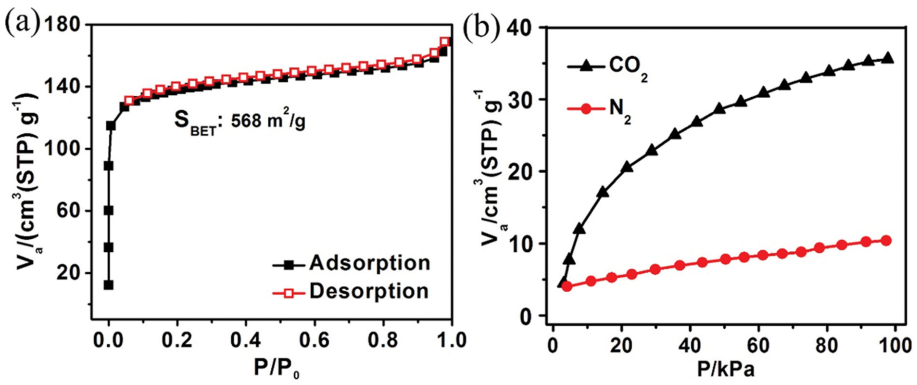

Fig. 2. (a) Nitrogen sorption isotherms at 77 K, 1 bar and (b) CO_2 and N_2 adsorption isotherms of ZIF-302 nanocrystals at 298 K, 1 bar.

Table 1. BET surface area and pore volume of ZIF-302 crystal

Samples	BET surface area m^2/g	Total pore volume cm^3/g	Micro-pore volume cm^3/g
ZIF-302	568	0.57	0.16

thesized crystals were activated and degassed under vacuum at 50 °C for 24 h before the adsorption-desorption test. As shown in Fig. 2(a), the low-temperature adsorption isotherm of ZIF-302 samples proved to be the I-type adsorption and there was no hysteresis. The rate of crystal adsorption increases rapidly at lower pressure, which is attributed to the existence of micropores. Moreover, the adsorption isotherm also presents a continuously rising platform due to the significant outer region of agglomerated particles [33]. In addition, the BET surface area of ZIF-302 crystal was calculated as 568 m^2/g. The total pore and micropore volume were 0.57 and 0.16 cm^3/g, respectively (Table 1), which are higher than that samples reported in the literature [23]. The results were mainly due to the smaller size of as-synthesized ZIF-302 nanoparticles. The above results indicate that ZIF-302 possess large specific surface area and pore volume.

The solubility of gas in ZIF-302 can be measured by isothermal pressure swing adsorption. Therefore, the adsorption isotherms of CO_2 and N_2 on ZIF-302 samples at pressure of 0-100 kPa and temperature of 25 °C were tested by static volume method (Fig. 2(b)). The steepness of the low-pressure slope in the CO_2 isotherm indicates that the affinity between CO_2 and ZIF-302 nanocrystals is high, while the N_2 isotherm shows a strong linear relationship, indicating that the interaction between N_2 and ZIF-302 is weak. When the two gases reach adsorption saturation at atmospheric pressure, the difference of adsorption capacity clearly shows the high adsorption selectivity of CO_2/N_2. These results indicate that ZIF-302 as a potential candidate filler has important research significance in the future preparation of MMMs for CO_2/N_2 separation.

2. Synthesis and Analysis of ZIF-302/P84 MMMs

The characterization and analysis of the synthesized ZIF-302/P84 MMM was conducted through various physical and chemical techniques. Fig. 3(a) shows the XRD patterns of pure P84 and ZIF-302/P84 mixed matrix membranes. A typical broad peak ranging from 14° to 32° was observed in the pure P84 membrane, indicating its amorphous structure. Note that sharp characteristic diffraction peaks of ZIF-302 appear in ZIF-302/P84 MMMs and the intensity increases with particle loading. These results indicate that the structure of ZIF-302 nanoparticles is maintained during the synthesis of MMMs. Subsequently, the effect of the exact loading amount of inorganic filler on the thermal stability in the mixed matrix membrane was evaluated by TGA measurement. As shown in Fig. 3(b), we found that the weight loss of ZIF-302/P84 MMMs was only 15% between 40-300 °C, which was mainly derived from the removal of physically adsorbed water and structured water. All the membrane samples began to decompose above 400 °C in air atmosphere, which proved the favorable thermal stability of ZIF-302/P84 MMMs. The thermal decomposition process all occurred between 400-600 °C, and finally 50% of the initial weight of the membrane sample was maintained at 700 °C, which is related to the collapse of the crystal structure and the decomposition reaction of the P84 matrix [34].

To explore the interaction between ZIF-302 nanocrystals and P84 matrix, FTIR characterization analysis was performed on all synthesized samples. As shown in Fig. 4(a), the vibration peaks of the imide group in the P84 polymer are evident at 720, 1,089, 1,360 and 1,712 cm^{-1}, corresponding to the bending band of C=O, the stretching band of C-N-C, the stretching band of C=N, and the symmetric tensile band of C=O, respectively. The typical vibration peak with the combination of ZIF-302 and P84 appears at about 425 cm^{-1} in the mixed matrix membranes (Fig. 4(b)), assigned to the Zn-N bond between the imidazole and the metal of ZIF-302. The above results indicate that ZIF-302 nanoparticles were successfully doped into the P84 polymer matrix, and the intensity of the peak gradually increased with the particles loading. However, the absorption band peak between 1,712 and 1,089 cm^{-1} in the ZIF-302 based mixed matrix membrane sample decreased (Fig. 4(b)), which may have been due to the hydrogen bond interaction between the imide group of P84 and the imidazole of ZIF-

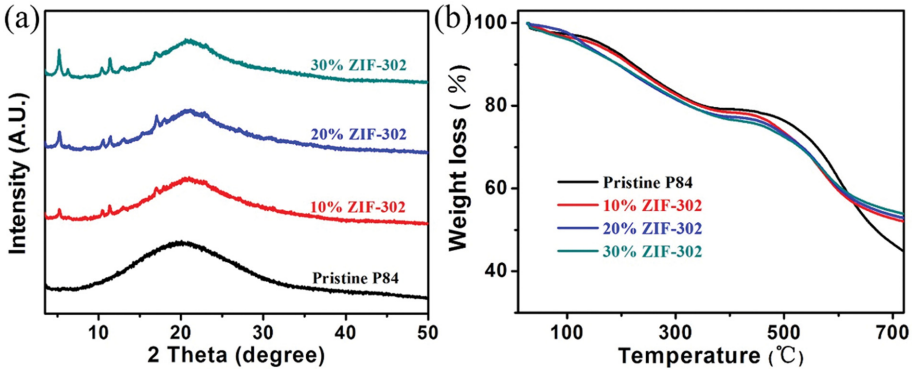

Fig. 3. (a) XRD patterns and (b) TGA curves of ZIF-302 nanocrystals, pristine P84 membrane and ZIF-302/P84 MMMs with various loadings in air atmosphere.

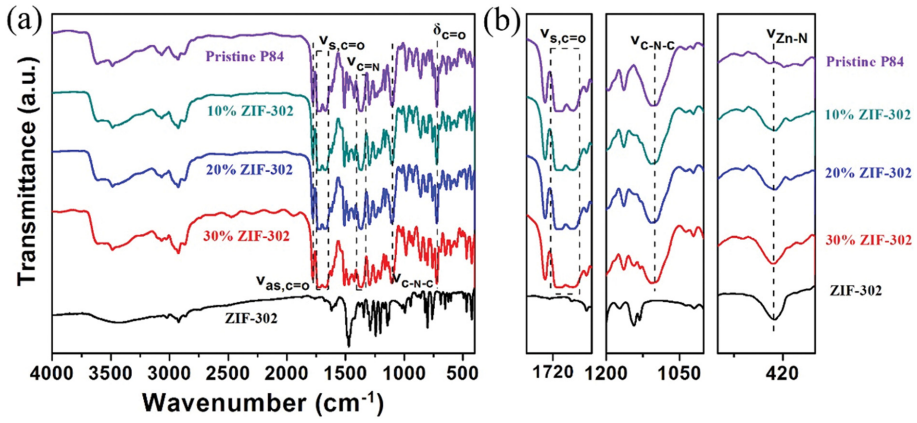

Fig. 4. (a) The whole and (b) local amplification of FTIR spectra of the pure ZIF-302 nanocrystals, pristine P84 membrane and ZIF-302/P84 MMMs.

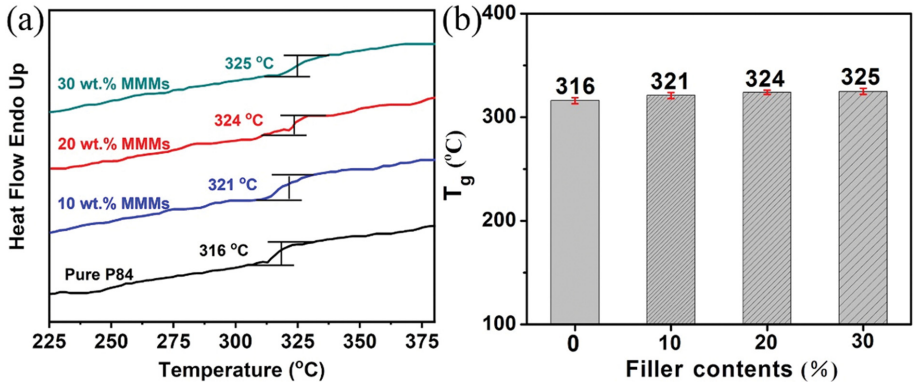

Fig. 5. (a) DSC curves and (b) glass transition temperature (T_g) of the pristine P84 membrane and MMMs with various contents of ZIF-302 nanocrystals.

302 crystals [35]. In addition, no peak vibration excursions were observed in the MMMs, indicating no chemical bond between the polymer chain and the filler.

The interfacial interaction between ZIF-302 and P84 substrates was further determined by DSC measurements. As shown in Fig. 5, the glass transition temperature (T_g) of the pure P84 membranes tested is 316 °C, which is well coincident with the value reported in the literature [36]. The gradual increase of fillers in P84 membranes resulted in the increase of T_g value, indicating that there is a good interaction between ZIF-302 and P84 matrix. On the one hand, this forward transfer may be due to reduced mobility and hardening of the polymer chain due to the polymer adsorption on the MOF surface [37]. On the other hand, it may also be owing to hydrogen bond interactions between ZIF-302 and P84 substrates, as previously confirmed by infrared FTIR spectrogram measurements (Fig. 4(b)).

By controlling the concentration of the casting solution, all the synthesized membranes had similar thickness. The high precision micrometer measurement was approximately 20±1 μm. The microscopic morphology of pure P84 membranes and ZIF-302/P84 MMMs was investigated by SEM characterization analysis. As shown in Fig. 6(a), the pure P84 matrix is defect-free with a highly smooth and uniform morphology. According to Fig. 6(b)-(d), it was found that ZIF-302 nanocrystals are uniformly distributed in the P84 matrix when the loading of ZIF-302 was 10-30 wt%. In addition, the appearance of the circular network morphology of the polymer is another evidence of strong interfacial interaction [38]. It can be seen from the higher magnification image (Fig. 6(e), (f))) that the ZIF-302 nanocrystals are well surrounded by the P84 matrix; no visible voids (such as "sieve in a cage") and obvious crystals are observed. As shown in the cross-sectional EDX mapping (Fig. 6(g), (h)), there are no agglomerated ZIF-302 nanocrystals (red: Zn signal) in the P84 polymer matrix when the loading of ZIF-302 is 20% and 30 wt%. The results further prove that the introduction of ZIF-302 at higher loadings of 30 wt% did not lead to particle aggregation or clustering. The above results prove that there is good adhesion between the P84 polymer and ZIF-302 filler.

3. Gas Permeation of ZIF-302/P84 MMMs

To clarify the effect of ZIF-302 loading, the separation performance of pure P84 membrane and ZIF-302/P84 mixed matrix membrane was tested by using Wicke-Kallenbach technology to separate equimolar CO_2/N_2 mixture. The feed pressure and operating temperature were fixed as 3 bar and 60 °C, respectively. As shown in Fig. 7, the CO_2 permeability and separation factor of the pure P84 membrane were 0.87 Barrer and 17, which are almost

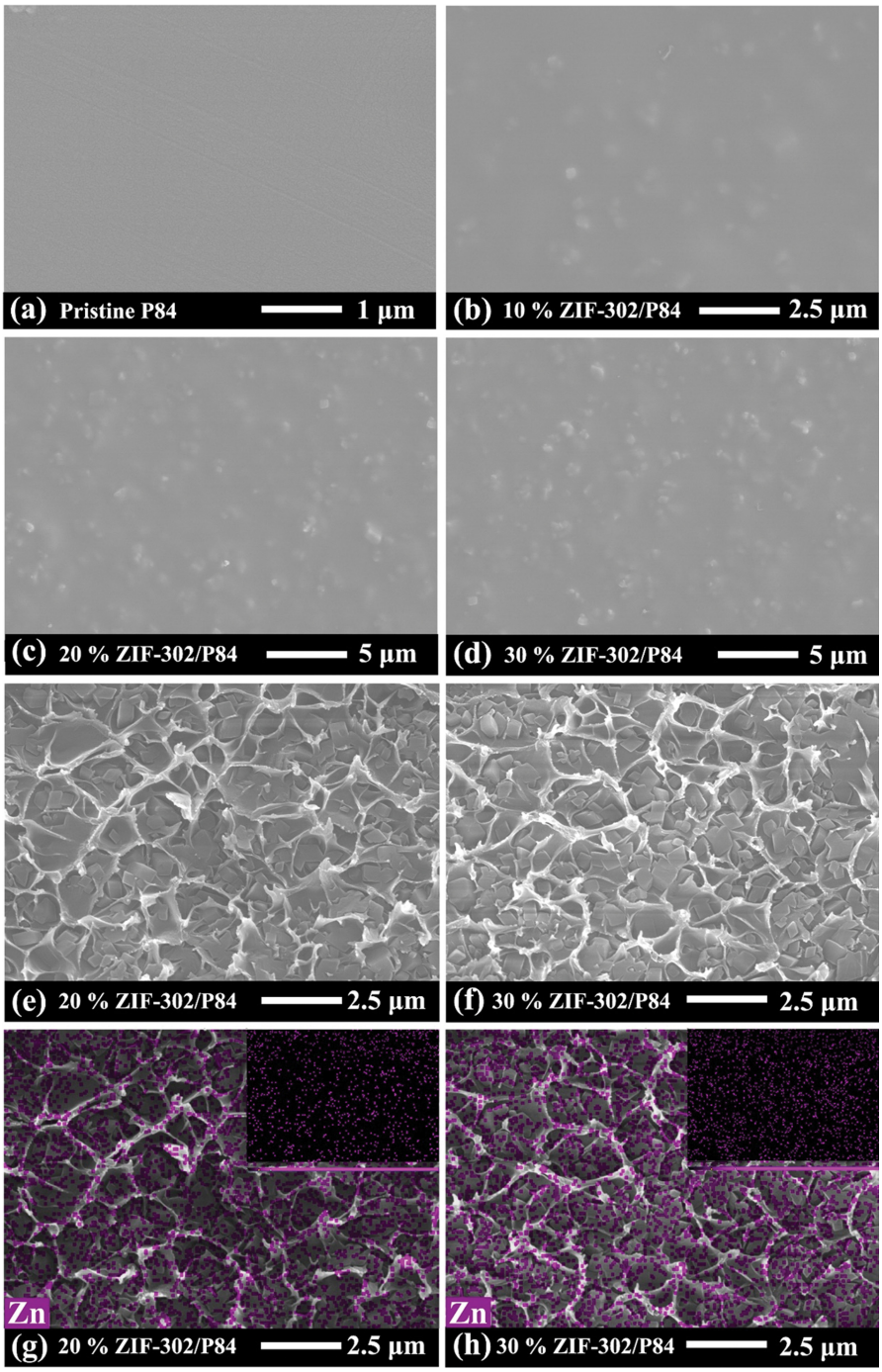

Fig. 6. SEM images of (a) pristine P84 membrane, (b) 10 wt%, (c), (e) 20 wt% and (d), (f) 30 wt% ZIF-302/P84 MMMs. The cross-sectional EDX mapping of the (g) 20 wt% and (h) 30 wt% ZIF-302/P84 MMMs.

consistent with the results of previous studies [39]. In addition, the CO_2 permeability of ZIF-302/P84 MMMs increased from 0.87 to 5.2 Barrer with the increase of ZIF-302 loading, which increased by nearly five times. Furthermore, the N_2 permeability showed a slight decrease, indicating that the selectivity of CO_2/N_2 increased by 170% (from 17 to 46). Interestingly, when the CO_2 concentration in the feed gas was reduced from 50% to 10%, the permeability of CO_2 and the separation factor of CO_2/N_2 were improved compared with 50% CO_2 (Fig. 7). The results show that the selective adsorption and diffusion effects are amplified due to the good interaction between carbon dioxide and framework of ZIF-302 crystals [16]. The enhancement of adsorption and diffusion effect is mainly due to the preferential adsorption of CO_2 by ZIF-302 nanocrystals (Fig. 2). Furthermore, the preferential adsorption of CO_2 in MMMs further hinders the diffusion of N_2. Therefore, both CO_2 adsorption and diffusion effects are enhanced, which improves the separation performance of MMMs. We further investigated the effects of feed pressure on the separation performance of the pure

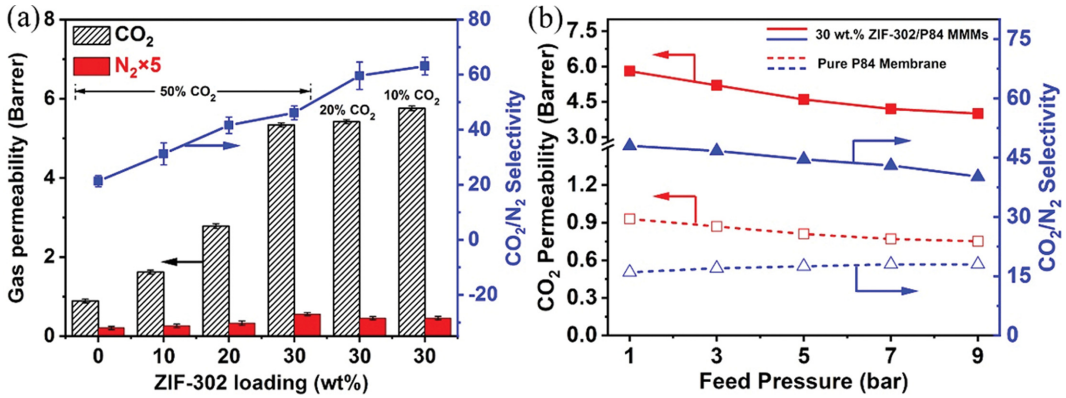

Fig. 7. (a) The gas permeation results of the pure P84 membranes and MMMs with different ZIF-302 particle loadings for the CO_2/N_2 (1 : 1) mixture at 3 bar and 60 °C. The -% is CO_2 concentration in the feed gas. (b) The separation performance of the pure P84 membrane and 30 wt% ZIF-302/P84 MMMs for CO_2/N_2 mixtures (1 : 1) as a function of the feed pressure at 60 °C.

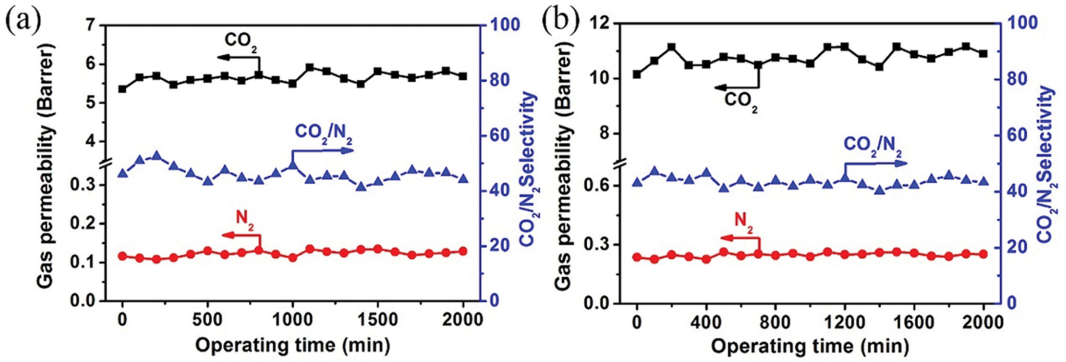

Fig. 8. Long-term operation test of the gas permeability and CO_2/N_2 selectivity for 30 wt% ZIF-302/P84 membranes at 3 bar and 60 °C: (a) Dry gases and (b) humidified gases.

P84 membrane and 30 wt% ZIF-302/P84 MMMs for CO_2/N_2 mixtures (1 : 1) at 60 °C. As shown in Fig. 7(b), the CO_2 permeability of pure P84 membrane only decreased by 19% with increasing feed pressure, while the CO_2 permeability of MMMs decreased gradually from 5.8 to 4 barrer, decreasing by 31%. Simultaneously, the separation factor of MMMs for CO_2/N_2 mixture also decreased from 48 to 40.2, while the separation factor of pure P84 membrane gradually increased by 12%. Therefore, the permeability decreased in pure P84 and MMMs with increasing feed pressure up to 9 bar, which is consistent with the dual-mode behavior in glassy polymers [40]. In addition, no signs of induced plasticization were observed within the pressure range studied.

4. Long-term Operation Stability Test

Furthermore, the gas permeation of 30 wt% ZIF-302/P84 MMMs was examined with equal ratio of CO_2/N_2 (1 : 1) under dry and wet gas feed. As shown in Fig. 8, the prepared MMMs also showed reliable long-term operational stability. The results show that the separation performance of CO_2/N_2 mixture was stable for more than 30 h at 3 bar and 60 °C, and the separation selectivity was maintained at about 40 for both dry gas and wet gas. Compared with dry gas, we found that the gas permeability of pure P84 membranes and ZIF-302/P84 MMMs was significantly increased, while the membrane selectivity was not obviously changed under the humidification condition (Relative humidity was about 30%). This phenomenon may be owing to water induced membrane expansion [41]. In addition, the stability of all synthesized membranes was investigated by immersing in water at 35 °C for 24 to 48 h, and then drying in vacuum at 100 °C for 24 h. The gas permeation results are listed in Table 2. The results show that separation factor of the ZIF-302/P84 MMMs for CO_2/N_2 was still as high as 38 after soaking in water for 48h. Although the separation factor of the CO_2/N_2 showed a slight decrease, it still maintained a higher separation performance. The ZIF-302/P84 MMMs have excellent attractiveness for separation of CO_2/N_2 combined with good separation performance, which can be potentially used in industrial applications.

Table 2. The separation performance of as-synthesized membranes was immersed in water in water at different soak time

Soak time (h)	Permeability (Barrer)		SF (CO_2/N_2)
	CO_2	N_2	
0	5.5	0.11	50
24	5.8	0.14	42
48	5.7	0.15	38

CONCLUSIONS

High-quality ZIF-302/P84 MMMs with good CO_2/N_2 separation performance and hydrothermal stability were successfully prepared by dispersing ZIF-302 crystals uniformly in P84 matrix for the first time. The size of ZIF-302 crystals was effectively reduced (~200 nm) to be suitable for the preparation of MMMs by introducing a modulator. On the one hand, the stability of MMMs prepared by ZIF-302 nanoparticles with super-hydrophobicity as inorganic filler is higher, which the separation performance was maintained more than 48 h immersing in water. On the other hand, the addition of 30 wt% ZIF-302 nanocrystals into the polymer matrix significantly improved the CO_2 permeability and the CO_2/N_2 separation selectivity by 497% and 170%, respectively, compared to the pure P84 membrane. In addition, the long-term operation stability showed that the P84 membrane filled with 30 wt% ZIF-302 particles still exhibited excellent CO_2/N_2 separation performance under wet gases. Therefore, our work confirms the potential of ZIF-302 for developing high-performance mixed-matrix membrane that could be promising for CO_2 capture.

ACKNOWLEDGEMENTS

This work was supported by the National Natural Science Foundation of China (21776124), Jiangsu Provincial NSFC (BK20171459), Foundation of Jiangsu Educational Committee of China (17KJA 530004), Jiangsu Province Key Laboratory of Fine Petrochemical Engineering. Y.P. also appreciates the support from the Six Talent Peaks Project and Qing-Lan Engineering Project of Jiangsu Province.

REFERENCES

1. J. Liu, P. K. Thallapally, B. P. McGrail, D. R. Brown and J. Liu, *Chem. Soc. Rev.*, **41**, 2308 (2012).
2. Z. W. Ma, P. Zhang, H. S. Bao and S. Deng, *Renew. Sust. Energ. Rev.*, **53**, 1273 (2016).
3. F. R. Service, *Science*, **305**, 962 (2004).
4. L. M. Robeson, *J. Membr. Sci.*, **320**, 390 (2008).
5. B. Ghalei, K. Sakurai, Y. Kinoshita, K. Wakimoto, A. P. Isfahani, Q. Song, K. Doitomi, S. Furukawa, H. Hirao, H. Kusuda, S. Kitagawa and E. Sivaniah, *Nat. Energy*, **2**, 17086 (2017).
6. N. C. Su, D. T. Sun, C. M. Beavers, D. K. Britt, W. L. Queen and J. J. Urban, *Energ. Environ. Sci.*, **9**, 922 (2016).
7. M. J. C. Ordonez, K. J. Balkus Jr., J. P. Ferraris and I. H. Musselman, *J. Membr. Sci.*, **361**, 28 (2010).
8. C. A. Dunn, Z. Shi, R. Zhou, D. L. Gin and R. D. Noble, *Ind. Eng. Chem. Res.*, **58**, 4704 (2019).
9. D. Zhao, J. Ren, H. Li, K. Hua and M. Deng, *J. Energy Chem.*, **23**, 227 (2014).
10. D. Zhao, J. Ren, H. Li, X. Li and M. Deng, *J. Membr. Sci.*, **467**, 41 (2014).
11. J. Zhao, K. Xie, L. Liu, M. Liu, W. Qiu and P. A. Webley, *J. Membr. Sci.*, **583**, 23 (2019).
12. T. Yang, Y. Xiao and T. S. Chung, *Energ. Environ. Sci.*, **4**, 4171 (2011).
13. B. Zornoza, A. Martinez-Joaristi, P. Serra-Crespo, C. Tellez, J. Coronas, J. Gascon and F. Kapteijn, *Chem. Commun.*, **47**, 9522 (2011).
14. B. Seoane, J. Coronas, I. Gascon, M. Etxeberria Benavides, O. Karvan, J. Caro, F. Kapteijn and J. Gascon, *Chem. Soc. Rev.*, **44**, 2421 (2015).
15. S. Kim, E. Shamsaei, X. Lin, Y. Hu, G. P. Simon, J. G. Seong, J. S. Kim, W. H. Lee, Y. M. Lee and H. Wang, *J. Membr. Sci.*, **549**, 260 (2018).
16. T. H. Bae, J. S. Lee, W. L. Qiu, W. J. Koros, C. W. Jones and S. Nair, *Angew. Chem. Inter. Ed.*, **49**, 9863 (2010).
17. A. Sabetghadam, B. Seoane, D. Keskin, N. Duim and J. Gascon, *Adv. Funct. Mater.*, **26**, 3154 (2016).
18. M. Askari and T. S. Chung, *J. Membr. Sci.*, **444**, 173 (2013).
19. J. E. Ba Chman, Z. P. Smith, L. Tao, T. Xu and J. R. Long, *Nat. Mater.*, **15**, 845 (2016).
20. C. Zhang, K. Zhang, L. Xu, Y. Labreche, B. Kraftschik and W. Koros, *AIChE J.*, **60**, 2625 (2014).
21. T. Li, Y. Pan, K. V. Peinemann and Z. Lai, *J. Membr. Sci.*, **425**, 235 (2013).
22. L. Xiang, Y. Pan, G. Zeng, J. Jiang and C. Wang, *J. Membr. Sci.*, **500**, 66 (2016).
23. N. Nguyen, H. Furukawa, F. Gándara, H. T. Nguyen, K. E. Cordova and O. M. Yaghi, *Angew. Chem. Inter. Edit.*, **53**, 10645 (2014).
24. M. Sarfraz and M. Ba-Shammakh, *Arab. J. Sci. Eng.*, **36**, 154 (2016).
25. X. Qiao and T. S. Chung, *Ind. Eng. Chem. Res.*, **44**, 8938 (2005).
26. N. Nguyen, H. Furukawa, F. Gándara, H. T. Nguyen, K. E. Cordova and O. M. Yaghi, *Angew. Chem. Inter. Edit.*, **53**, 10645 (2014).
27. L. Xiang, Y. Pan, J. Jiang, Y. Chen, J. Chen, L. Zhang and C. Wang, *Chem. Eng. Sci.*, **160**, 236 (2017).
28. S. Kelman, H. Lin, E. S. Sanders and B. D. Freeman, *J. Membr. Sci.*, **305**, 57 (2007).
29. A. Car, C. Stropnik, W. Yave and K. V. Peinemann, *Sep. Purif. Technol.*, **62**, 110 (2008).
30. M. Sarfraz and M. Ba Shammakh, *J. Ind. Eng. Chem.*, **36**, 154 (2016).
31. J. Cravillon, C. Schroder, H. Bux, A. Rothkirch, J. Caro and M. Wiebcke, *Crystengcomm*, **14**, 492 (2012).
32. X. Wu, Y. Yang, X. Lu and Z. Wang, *J. Membr. Sci.*, **613**, 118518 (2020).
33. M. Fang, C. Wu, Z. Yang, W. Tao, X. Yang and J. Li, *J. Membr. Sci.*, **474**, 103 (2015).
34. W. H. Lin, R. H. Vora and T. S. Chung, *J. Polym. Sci. Pol. Phys.*, **38**, 2703 (2015).
35. B. Ghalei, K. Sakurai, Y. Kinoshita, K. Wakimoto, A. Isfahani, Q. Song, K. Doitomi, S. Furukawa, H. Hirao and H. Kusuda, *Nat. Energy*, **2**, 17086 (2017).
36. A. Guo, Y. Ban, K. Yang and W. Yang, *J. Membr. Sci.*, **562**, 76 (2018).
37. N. C. Su, D. T. Sun, C. M. Beavers, D. K. Britt, W. L. Queen and J. J. Urban, *Energ. Environ. Sci.*, **9**, 922 (2016).
38. M. Ordo Ez, K. J. Balkus, J. P. Ferraris and I. H. Musselman, *J. Membr. Sci.*, **361**, 28 (2010).
39. A. C. Lua and Y. Shen, *J. Appl. Polym. Sci.*, **128**, 4058 (2013).
40. J. Ploegmakers, S. Japip and K. Nijmeijer, *J. Membr. Sci.*, **428**, 445 (2013).
41. S. Shishatskiy, J. R. Pauls, S. P. Nunes and K. V. Peinemann, *J. Membr. Sci.*, **359**, 44 (2010).